Ionization Energies of Acridine, Phenazine, and Diazaphenanthrenes

O. Dolgounitcheva, V. G. Zakrzewski, and J. V. Ortiz*

Department of Chemistry, Kansas State University, Manhattan, Kansas 66506-3701

Received: June 11, 1997; In Final Form: August 22, 1997[⊗]

Ab initio electron propagator calculations on the lowest vertical ionization energies of acridine, phenazine, and five diazaphenanthrene isomers have been performed with the partial third order and outer valence Green's function approximations of electron propagator theory. Agreement with photoelectron spectra is very close, enabling the clarification of previous assignments. Numerous misorderings of final states from Koopmans's theorem are revealed. With the present approximations, Feynman−Dyson amplitudes are equivalent to canonical molecular orbitals. Plots of these one-electron functions aid in the interpretation of the spectra by revealing patterns of localization. Many final-state holes exhibit considerable mixing between nitrogen, lone-pair hybrids, and σ-bonding lobes.

Introduction

Aza and diaza derivatives of polycyclic aromatic hydrocarbons possess unique chelating properties, display extensive biological activity, and are widely used in analytical chemistry, pharmacology,[1−5] and molecular biology.[6] These molecules have been thoroughly scrutinized for antitumor activity,[7] carcinogenicity, and mutagenicity.[8] The ability of some phenanthrolines (diazaphenanthrenes) to inhibit electron transfer in biological systems has attracted attention.[9] Derivatives of acridine and phenanthrolines have been studied for their potential antiviral (including anti-HIV) properties.[10]

Such chemical activity may correlate with molecular properties such as ionization energies and related orbital structures.[11] These relationships are not yet founded on reliable data, for heterocycles of this size have been examined only with semiempirical calculations or with ab initio methods employing small basis sets.[12]

Recently, a comprehensive electron propagator study on photoelectron spectra of three polycyclic aromatic hydrocarbons has appeared[13] in which detailed results for anthracene, phenanthrene, and naphthacene were given and excellent agreement with experiment was achieved. While there are abundant data for these parent molecules, only one study exists on photoelectron spectra of aza and diaza derivatives of anthracene and phenanthrene.[14] The spectra presented in that work contain a number of unresolved, poorly resolved, or overlapping bands. Assignments were made on the basis of semiempirical calculations.

Ionization energies from molecules with adjacent nitrogen lone pairs usually are assigned with the aid of a simple, two-level splitting model. Here, two lone-pair hybrids produce two combinations, the out-of-phase σN_- and the in-phase σN_+. Relative positions are determined by "through-space" or "through-bond" interactions.[14,15] Photoelectron spectra of molecules with two aza centers usually are assumed to have two bands corresponding to ionizations from nitrogen lone-pair orbitals.[14,16] Unfortunately, this concept may lead to erroneous assignments, especially when bands overlap.

Azabenzenes already have been investigated with electron propagator techniques.[17,18] Numerous final-state misorderings from Koopmans's theorem have been revealed. Even in the simplest case of pyridazine, there are four MOs with significant delocalization of nitrogen lone pairs into the aromatic core.[18] Thus, there is a need for an accurate theoretical description of heteropolycyclic compounds.

Methods

Electron propagator methods provide accurate interpretations and predictions of photoelectron spectra.[19−25] Final-state orbital relaxation and differential electron correlation are taken into account in calculations of vertical ionization energies and electron affinities. Propagator methods not only provide information on ionization energies but also yield Feynman−Dyson amplitudes, ϕ^{FDA}, where

$$\phi^{\mathrm{FDA}}(x_1) = \int \psi^*_{N-1}(x_2,x_3,x_4,...,x_N)\psi_N(x_1,x_2,x_3,...,x_N)\, dx_2\, dx_3\, dx_4 \ldots dx_N$$

These one-electron functions, also known as Dyson orbitals, are overlaps between initial states with N electrons and final states with $N - 1$ electrons. Pole strengths, p, are defined by

$$p = \int |\phi^{\mathrm{FDA}}(x_1)|^2\, dx_1$$

and are proportional to photoionization intensities.

Because the OVGF (outer valence Green's function)[25] and P3 (partial third order)[26] approximations used here assume the diagonal form of the propagator self-energy matrix in the canonical MO basis, the corresponding FDAs are identical to canonical MOs. Correlated photoionization intensities calculated with these propagator methods are scaled by pole strengths that are less than unity and greater than zero. The OVGF and P3 approximations remain valid only for outer valence ionization energies for which the pole strengths are greater than ~0.80. For outer valence ionization energies of closed-shell molecules, contributions to a given FDA from the Koopmans orbital in question generally dominate those of other canonical orbitals. Lowered pole strengths usually indicate enhanced shake-up character in final states. In the uncorrelated case, the Koopmans's theorem (KT) value corresponds to a pole strength equal to unity. For all states studied here, the pole strengths are sufficiently large to justify use of the OVGF and P3 methods. Therefore, orbital and state labels are used interchangeably.

All MOs except for ls-like core orbitals were included in electron propagator calculations performed with the cc-pVDZ basis.[27] (Total energies are listed in ref 28.) Hartree−Fock

[⊗] Abstract published in *Advance ACS Abstracts,* October 1, 1997.

S1089-5639(97)01910-5 CCC: $14.00

TABLE 1: Acridine Ionization Energies (eV)

MO	KT	OVGF *p*	P3 *p*	expt[14]	orbital type
$4b_1$	7.74	7.70	7.83	7.88	π_1
		0.88	0.87		
$3a_2$	8.55	8.45	8.65	8.69	π_2
		0.89	0.87		
$22a_1$	11.10	9.14	9.20	9.3	σN
		0.88	0.87		
$2a_2$	9.58	9.12	9.24	9.32	π_3
		0.88	0.86		
$3b_1$	11.36	10.47	10.56	10.59	π_4
		0.86	0.84		
$2b_1$	12.12	11.05	11.08	10.9	π_5
		0.85	0.83		
$18b_2$	13.45	11.69	11.83		σ
		0.88	0.88		
$17b_2$	13.72	12.00	12.09		σ
		0.88	0.88		
$1a_2$	13.60	12.22	12.18	11.97	π_6
		0.82	0.81		
$21a_1$	14.10	12.30	12.25		σ
		0.87	0.86		
$20a_1$	14.90	13.13	13.11		σ
		0.88	0.86		
$1b_1$	15.62	13.69	13.56	13.5	π_7
		0.76	0.76		
$19a_1$	15.73	13.76	13.79		σ
		0.87	0.86		
$16b_2$	16.02	13.87	14.00		σ
		0.87	0.86		

geometry optimizations on the neutral molecules were carried out with the 6-311G*[29] basis set using GAUSSIAN 94.[30] Three-dimensional plots and structural diagrams were generated with MOLDEN.[31] The 0.05 FDA contours are displayed in the orbital plots. Pole strengths are listed immediately beneath OVGF and P3 ionization energies in the tables.

Close agreement with experiment is generally obtained for closed-shell molecules with flexible basis sets.[26,32] Systematic employment of correlation-consistent basis sets[27] has been especially successful.[26] A semidirect algorithm for the OVGF[25] and P3 methods[26] was reported recently.[33] OVGF code is incorporated in GAUSSIAN 94[30] while P3 is implemented in a modified version of this program complex.

Results and Discussion

Figure 1 presents a numbering scheme for nuclei. Calculated vertical ionization energies and pole strengths (*p*) are collected in Tables 1−5 together with experimental data on 9-azaanthracene (acridine), 9,10-diazaanthracene (phenazine), 9,10-diazaphenanthrene (benzo[*c*]cinnoline or phenazone), 1,8-diazaphenanthrene (4,7-phenanthroline), and 4,5-diazaphenanthrene (1,10-phenanthroline). Tables 6 and 7 display predictions for 2,7-diazaphenanthrene (3,8-phenanthroline) and 3,6-diazaphenanthrene (2,9-phenanthroline).

Acridine. The lowest ionization state corresponds to a π MO, $4b_1$, with four nodal planes (Figure 2). This MO resembles the highest occupied molecular orbital or anthracene,[13] although electron density is less concentrated near nuclei 9 and 10. Both OVGF and P3 results are in very good agreement with experiment. A well-resolved, sharp feature with pronounced vibrational structure can be seen in the spectrum.[14] For anthracene, the corresponding P3 result is 7.31 eV.

The second ionization band corresponds to electron detachment from the π_2 orbital ($3a_2$), which seems to be an exact copy of its analog in anthracene. P3 calculations on anthracene produce an ionization energy of 8.46 eV for the analogous b_{1g} MO. A sharp peak at 8.69 eV was assigned to the lowest $^2A_2$ final state.

TABLE 2: Phenazine Ionization Energies (eV)

MO	KT	OVGF *p*	P3 *p*	expt[14]	orbital type
$2b_{2g}$	8.24	8.15	8.28	8.33	π_1
		0.88	0.87		
$2b_{1g}$	8.68	8.64	8.87	9.06	π_2
		0.89	0.87		
$12a_g$	10.80	8.76	8.99	9.2 ± 0.1	σN_+
		0.88	0.88		
$1a_u$	9.75	9.28	9.42	9.56	π_3
		0.88	0.86		
$10b_{1u}$	13.34	10.81	10.81	10.65 ± 0.2	σN_-
		0.86	0.85		
$2b_{3u}$	12.02	11.02	11.06	10.9	π_4
		0.84	0.82		
$1b_{2g}$	12.82	11.70	11.82	11.6	π_5
		0.85	0.84		
$10b_{2u}$	13.80	12.13	12.19		σ
		0.88	0.87		
$8b_{3g}$	14.00	12.17	12.34		σ
		0.88	0.87		
$1b_{1g}$	13.77	12.40	12.38	12.5	π_6
		0.81	0.80		
$11a_g$	14.50	12.72	12.71		σ
		0.87	0.86		
$9b_{1u}$	15.18	13.38	13.37		σ
		0.87	0.86		
$1b_{3u}$	16.32	14.26	14.18	14	π_7
		0.75	0.75		
$9b_{2u}$	16.41	14.20	14.36		σ
		0.87	0.86		

TABLE 3: Benzo[*c*]cinnoline Ionization Energies (eV)

MO	KT	OVGF *p*	P3 *p*	expt[14]	orbital type
$19b_2$	10.34	8.16	8.34	8.3 ± 0.3	σN_-
		0.87	0.86		
$3a_2$	8.54	8.45	8.65	8.69	π_1
		0.89	0.89		
$4b_1$	8.79	8.68	8.84	9.00	π_2
		0.89	0.87		
$2a_2$	10.08	9.59	9.81	9.84	π_3
		0.88	0.87		
$3b_1$	10.84	10.20	10.37	10.40	π_4
		0.88	0.86		
$21a_1$	13.18	11.19	11.41	10.85 ± 0.05	σ
		0.88	0.87		
$2b_1$	13.57	12.27	12.30	12.13	π_5
		0.83	0.81		
$18b_2$	13.96	12.26	12.32		σ
		0.88	0.88		
$1a_2$	13.91	12.44	12.41	12.65	π_6
		0.82	0.80		
$19a_1$	15.14	12.66	12.71	~12.7	σN_+
		0.86	0.84		
$20a_1$	14.58	12.88	12.92		σ
		0.88	0.87		
$17b_2$	15.03	13.27	13.26		σ
		0.88	0.87		
$1b_1$	16.37	14.44	14.39	14.30	π_7
		0.80	0.78		
$18a_1$	16.56	14.64	14.63		σ
		0.87	0.86		

Relative positions of the next two states have been assigned only tentatively. Although the OVGF and P3 results for the nitrogen lone-pair orbital ($22a_1$) and the π_3 MO ($2a_2$) have the opposite order, the absolute differences between these two values (0.02 and 0.04 eV, respectively) confirm their appearance as one overlapping band in the spectrum. In $22a_1$, there is extensive delocalization into nearby σ bond regions. $2a_2$ bears a strong resemblance to the $1a_u$ MO of anthracene; the corresponding P3 result for this final state was 9.09 eV.

Two $^2B_1$ states are predicted to follow. The π_4 MO ($3b_1$)

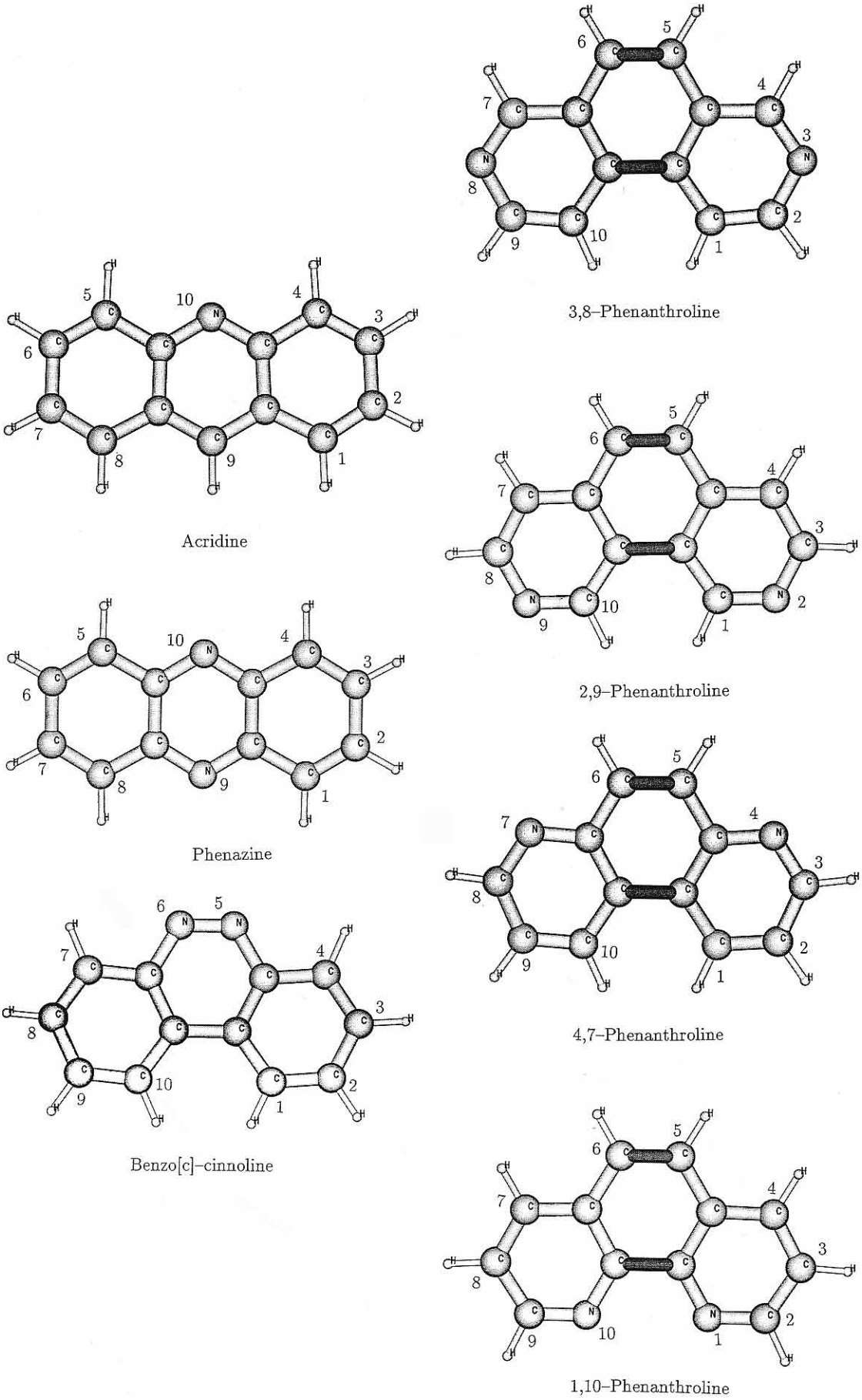

Figure 1. Atomic numbering schemes.

consists of three-center bonding patterns with alternating phases on each of the rings. For the sixth final state, a similar bonding pattern emerges, but on different nuclei. By forming symmetric and antisymmetric combinations of these two orbitals, it is

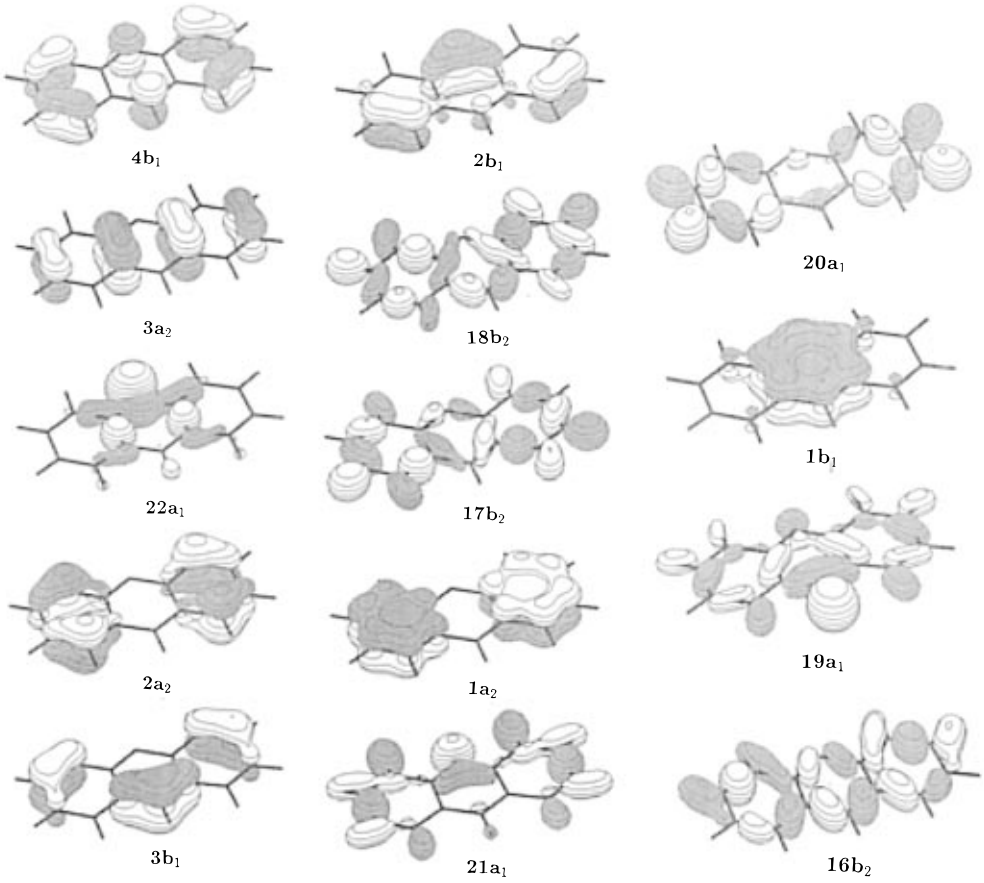

Figure 2. Acridine ionization energy FDAs (MOs).

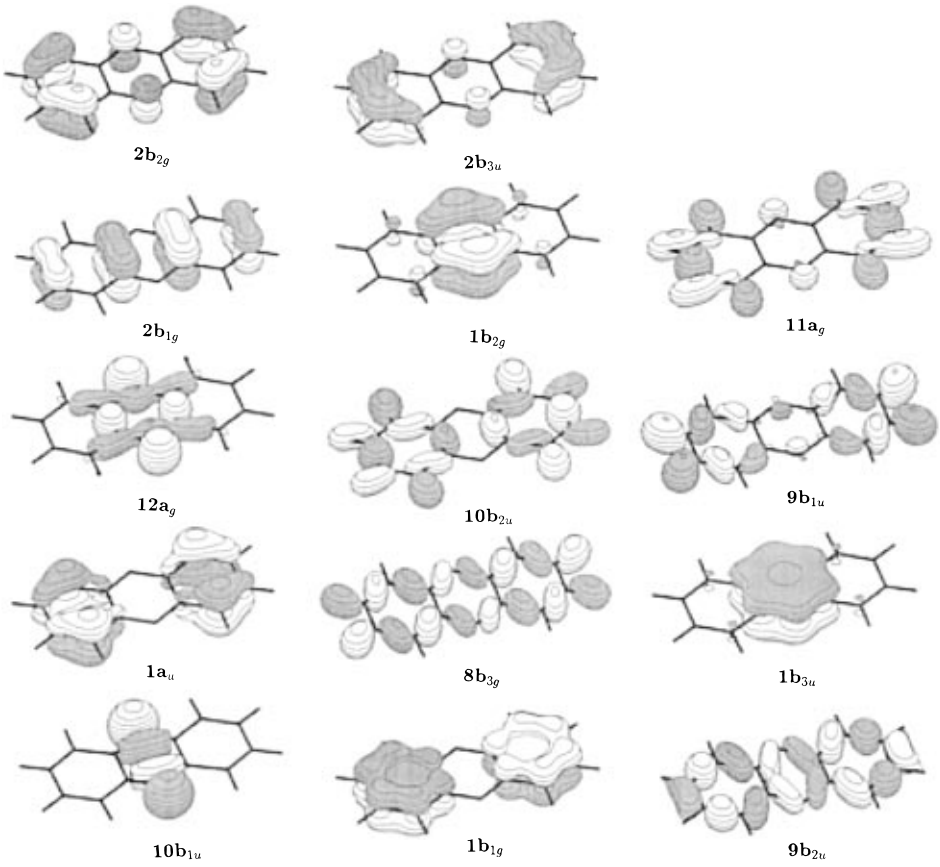

Figure 3. Phenazine ionization energy FDAs (MOs).

possible to recover patterns that resemble those of the corresponding anthracene π orbitals, $1b_{2g}$ and $2b_{3u}$. P3 ionization energies are 10.56 and 11.08 eV, respectively. Maxima in the spectrum occur at 10.59 and 10.9 eV; the areas beneath these

TABLE 4: 4,7-Phenanthroline Ionization Energies (eV)

MO	KT	OVGF *p*	P3 *p*	expt[14]	orbital type
$4b_1$	8.52	8.38	8.52	8.51	π_1
		0.89	0.88		
$3a_2$	8.56	8.53	8.73	8.86	π_2
		0.89	0.88		
$19b_2$	11.27	9.36	9.38	9.5 ± 0.05	σN_-
		0.88	0.87		
$21a_1$	11.39	9.44	9.43	9.5 ± 0.05	σN_+
		0.88	0.87		
$2a_2$	10.54	9.95	10.11	10.16	π_3
		0.88	0.86		
$3b_1$	11.66	10.85	11.00	10.84	π_4
		0.87	0.86		
$2b_1$	12.01	11.08	11.13	10.94	π_5
		0.85	0.86		
$18b_2$	13.88	12.11	12.19		σ
		0.88	0.87		
$20a_1$	14.29	12.45	12.60		σ
		0.89	0.88		
$1a_2$	14.79	13.19	13.09		π_6
		0.81	0.79		
$17b_2$	15.43	13.51	13.51		σ
		0.88	0.86		
$1b_1$	15.83	14.00	13.89		π_7
		0.80	0.80		
$19a_1$	15.85	13.93	13.93		σ
		0.88	0.87		
$16b_2$	16.07	14.25	14.17		σ
		0.88	0.86		

TABLE 5: 1,10-Phenanthroline Ionization Energies (eV)

MO	KT	OVGF *p*	P3 *p*	expt[14]	orbital type
$4b_1$	8.29	8.25	8.39	8.35	π_1
		0.89	0.88		
$3a_2$	8.62	8.49	8.67	8.6−8.7	π_2
		0.89	0.88		
$19b_2$	10.82	8.89	8.87	8.82	σN_-
		0.88	0.87		
$21a_1$	11.28	9.33	9.33	9.39 ± 0.05	σN_+
		0.88	0.87		
$2a_2$	10.62	10.02	10.17	10.11	π_3
		0.87	0.86		
$3b_1$	10.86	10.22	10.37	10.47	π_4
		0.87	0.85		
$2b_1$	12.49	11.45	11.47	11.16	π_5
		0.85	0.84		
$20a_1$	13.82	11.99	12.17	11.76 ± 0.05	σ
		0.89	0.88		
$18b_2$	14.30	12.53	12.60		σ
		0.88	0.87		
$1a_2$	14.41	12.87	12.78	12.36	π_6
		0.81	0.80		
$17b_2$	15.44	13.53	13.50		σ
		0.88	0.86		
$19a_1$	15.79	13.79	13.74		σ
		0.87	0.86		
$1b_1$	15.77	13.95	13.83		π_7
		0.80	0.79		
$16b_2$	15.77	13.93	13.89		σ
		0.87	0.86		

TABLE 6: 3,8-Phenanthroline Ionization Energies (eV)

MO	KT	OVGF *p*	P3 *p*	orbital type
$4b_1$	8.23	8.25	8.42	π_1
		0.89	0.88	
$3a_2$	9.53	9.09	9.39	π_2
		0.89	0.87	
$21a_1$	11.37	9.44	9.46	σN_+
		0.88	0.87	
$19b_2$	11.59	9.58	9.53	σN_-
		0.87	0.86	
$2a_2$	9.98	9.54	9.78	π_3
		0.88	0.87	
$3b_1$	11.50	10.75	10.92	π_4
		0.88	0.86	
$2b_1$	12.81	11.74	11.79	π_5
		0.85	0.83	
$18b_2$	13.50	11.81	12.00	σ
		0.89	0.88	
$1a_2$	14.87	13.28	13.20	π_6
		0.81	0.79	
$20a_1$	14.91	13.19	13.25	σ
		0.88	0.87	
$19a_1$	15.43	13.16	13.35	σ
		0.87	0.86	
$17b_2$	15.49	13.73	13.72	σ
		0.88	0.87	
$1b_1$	15.84	14.02	13.95	π_7
		0.80	0.79	
$18a_1$	16.39	14.33	14.43	σ
		0.88	0.86	

TABLE 7: 2,9-Phenanthroline Ionization Energies (eV)

MO	KT	OVGF *p*	P3 *p*	orbital type
$3a_2$	8.48	8.46	8.65	π_1
		0.89	0.88	
$4b_1$	8.92	8.73	8.87	π_2
		0.89	0.88	
$19b_2$	11.28	9.36	9.36	σN_-
		0.88	0.87	
$21a_1$	11.47	9.48	9.46	σN_+
		0.88	0.86	
$2a_2$	10.76	10.14	10.35	π_3
		0.88	0.86	
$3b_1$	10.90	10.25	10.46	π_4
		0.88	0.86	
$2b_1$	12.96	11.88	11.94	π_5
		0.85	0.83	
$20a_1$	14.08	12.32	12.48	σ
		0.89	0.88	
$18b_2$	14.31	12.43	12.52	σ
		0.88	0.87	
$1a_2$	14.77	13.19	13.09	π_6
		0.81	0.79	
$17b_2$	14.82	13.06	13.14	σ
		0.88	0.87	
$1b_1$	15.82	14.00	13.93	π_7
		0.80	0.79	
$19a_1$	16.00	13.82	13.96	σ
		0.87	0.86	
$18a_1$	16.57	14.62	14.64	σ
		0.87	0.86	

peaks are approximately equal. In the former feature, there is a shoulder at 10.44 eV, which was assigned to the π_4 final state. The peak at 10.59 eV was assigned to the π_5 final state. The computational methods used here seldom give an error of 0.49 eV for a π final state. A revised assignment therefore is made here: the maxima at 10.59 and 10.9 eV correspond to the π_4 and π_5 final states.

Ionization from a σ orbital, $18b_2$, is predicted at 11.8 eV. The calculated position of the following π_6 $^2A_2$ state is in good agreement with the experimental assignment. A broad feature from 11.4 to 12.4 eV displays a maximum at 11.97 eV that was assigned to the π_6 final state. A low pole strength for the $^2A_2$ state (0.81) suggests shake-up structure at higher energies. Koopmans's theorem predicts the wrong order of this π level and the next σ level, $17b_2$. The ionization energy from the next σ level, $21a_1$, is predicted to be only 0.07 eV higher than that of the π_6 MO. The overlapped feature at 11.4−12.4 eV contains contributions from all of these final states.

A prominent, unassigned peak at 12.9 eV in the experimental spectrum can be assigned to an MO ($20a_1$) that is delocalized

over C−H and C−C bonds. P3 and OVGF energies are 13.11 and 13.13 eV, respectively.

There is rather good agreement between P3 and experimental values for the highest π level. The corresponding MO is delocalized over six atoms of the central ring. A very low pole strength (0.76) predicts substantial shake-up structure for this final state. The higher lying $^2A_1$ state provides sufficient overlapping to further obscure the experimental feature at 13.5−13.8 eV. The last ionization described here is predicted to have an energy of 14.00 eV and to correspond to another σ-type MO, $16b_2$.

Phenazine. With the presence of another nitrogen atom in a position para to the first, there is a substantial shift to higher ionization energies except for states corresponding to lone-pair MOs. The first final state corresponds to a π MO, $2b_{2g}$, that displays the same nodal pattern as its counterparts for acridine and anthracene.[13] Agreement of experimental[14] and calculated values is very good for OVGF and is excellent for P3. A sharp peak followed by well-resolved vibrational structure is observed. Phenazine's lowest ionization energy is larger than acridine's.

The second ionization band is the result of overlap of two very close-lying ionized states, a $^2B_{1g}$ π state and a ^2A_g σ state corresponding to an in-phase combination of nitrogen lone-pair lobes (Figure 3). $12a_g$ exhibits considerable delocalization into the central ring's σ regions and into adjacent C−C bond regions. It is not obvious from the spectra which ionization energy is lower. Both OVGF and P3 predict that the π_2 ionization is lower.

The next ionization peak is very well resolved and corresponds to a π_3 ($1a_u$) MO with four lobes localized at the 1−2, 3−4, 5−6, and 7−8 bonds for the two external rings. Closer agreement with experiment is obtained for P3 than for OVGF.

The position of the π_4 ionization is not specified in the experimental spectrum due to its overlapping with the adjacent σ state and the very complicated structure of a broad feature at 10.5−11.2 eV. Our calculations place this ionization at 11.1 eV and predict that it is preceded by ionization from the out-of-phase combination of nitrogen lone-pair hybrids. Both OVGF and P3 energies for the latter state coincide with the experimental position within experimental error. The $10b_{1u}$ MO is chiefly an antisymmetric combination of N lone-pair hybrids with no contributions from other centers.

The following order is therefore predicted for the first six ionizations: $^2B_{2g}$ (π_1), $^2B_{1g}$ (π_2), ^2A_g (σN_+), ^2A_u (π_3), $^2B_{1u}$ (σN_-), and $^2B_{3u}$ (π_4).

The position of the next state, $^2B_{2g}$, was not defined properly in the experimental work.[14] There is an evident discrepancy between the π_5 placement in Figure 4 of ref 14 and the energy value given in Table 2 of ref 14. Our OVGF and P3 values of 11.70 and 11.82 eV correspond rather well with the position of a peak seen at 11.6−11.8 eV in the experimental spectrum. $1b_{2g}$ has two three-center, π-bonding lobes centered on the nitrogens that are significantly more localized than their anthracene counterparts of ref 13.

Ionizations from two close-lying σ MOs, $10b_{2u}$ and $8b_{3g}$, precede the π_6 ionization. Koopmans's theorem obtains the wrong order. Both σ MOs exhibit delocalized patterns of C−C and C−H σ-bonding lobes. These σ states correspond to a plateau between 12.0 and 12.5 eV.

The π_6 ionization energy of 12.4 eV is in close agreement with the tentative experimental value, 12.5 eV. A low pole strength for this ionization, 0.80, predicts the existence of shake-up states, which seems to be typical for symmetric, bonding π MOs.[13,17,34−36]

Another σ state, ^2A_g, is close to the π_6 level, $11a_g$. The corresponding MO includes a small contribution from nitrogen lone-pair hybrids while consisting mostly of C−C, C−H σ-bonding lobes.

The next ionization occurs from a σ MO, $9b_{1u}$, and corresponds to an unassigned feature at 13.0−13.4 eV in the experimental spectrum.

The highest π ionization state, $^2B_{3u}$, is placed at 14.2 eV by the calculations and at 14 eV in ref 14. The low pole strength value predicts shake-up structure at higher energies, and overlapping with a close-lying $^2B_{2u}$ state is possible.

Benzo[*c*]cinnoline. The adjacency of the two nitrogens produces unique orbital and energy patterns in this molecule. The first ionization occurs from an out-of-phase combination of lone-pair hybrids on two adjacent nitrogen atoms. Experiment places this ionization band at ∼8.3 eV. Our P3 result is in excellent agreement with this value. The corresponding $19b_2$ MO is predominantly localized in the vicinity of the N−N bond, although some delocalization over adjacent C−C bonds is evident. Antibonding interactions between the N-centered lobes produce a lower ionization energy for $19b_2$ than for the $19a_1$ MO (see below) that exhibits a bonding interaction between lone-pair hybrids.

Correlation corrections to Koopmans's theorem are large and cause a reordering of final states. Two of these states, π_1 and π_2, overlap with the σN_- level to provide a broad featureless band with a prominent maximum at ∼8.7 eV corresponding to ionization from the π_1 $3a_2$ MO. The agreement of the P3 energy and the experimental value is very close. The first π level in benzo[*c*]cinnoline corresponds to the second π level in phenanthrene according to symmetry and the pattern of delocalization.[13] The third state corresponds to electron detachment from a π_2 $4b_1$ MO and its position in the experimental spectrum is only tentatively given at 9 eV. Our P3 result, 8.84 eV, is close. The MO is very similar to the first π level of phenanthrene. This reversal of the first two π levels was mentioned as a possibility in ref 14. It is evident now that the presence of two adjacent nitrogen atoms in an aromatic molecule not only shifts the ionization potentials to higher energies but also leads to inversion of some levels compared with the parent hydrocarbon molecule.

The next ionization peak at 9.84 eV is well-resolved, and our P3 value of 9.81 eV is in excellent agreement with experiment. The corresponding π MO, $2a_2$, has four two-center lobes localized mostly on the external rings, with a small nitrogen contribution. This pattern is similar to the corresponding a_2 MO in phenanthrene.

Agreement with experiment for the π_4 state is excellent for P3. A strong resemblance exists between the $3b_1$ MO and its phenanthrene counterpart.

There is a significant discrepancy between the present calculations and the experimental assignment of ionization from a σN_+ combination of nitrogen lone-pair hybrids. Reference 14 places the corresponding energy at 10.85 eV. A broad feature of low intensity with an evident shoulder at 11.2−11.4 eV can be seen in the experimental spectrum. Our calculations put this cationic state, $^2A_1$, at 11.19 eV (OVGF) and 11.41 eV (P3); the FDA corresponds to a delocalized σ pattern with only small contributions from nitrogen lone-pair hybrids (Figure 4). This MO has evident bonding character. Significant geometry changes must occur upon ionization, and this band represents the onset of ionization from σ MOs.

The following two cationic states, $^2B_1$ and $^2B_2$, have very close energies and underlie an overlapping band at ∼12.3 eV. Delocalized π bonding characterizes the former: there is a node between the nitrogens and the rest of the molecule. This state

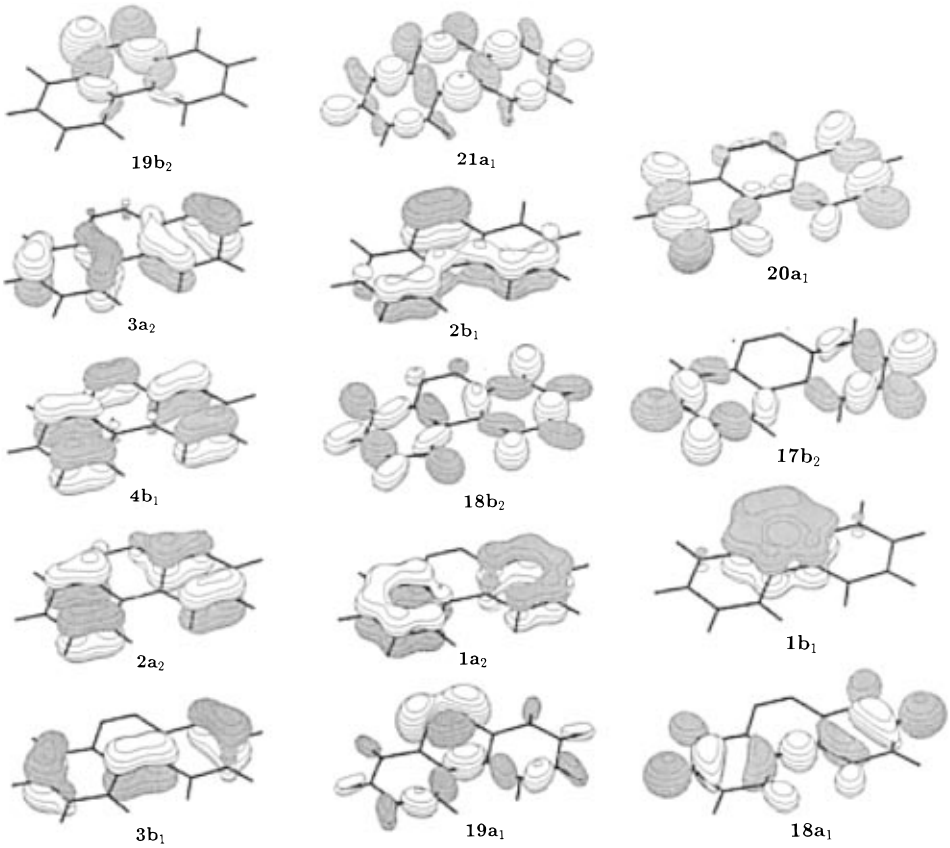

Figure 4. Benzo[*c*]cinnoline ionization energy FDAs (MOs).

has a low pole strength, which implies the presence of shake-ups under the envelope at 12−13.5 eV. The close-lying σ MO, $18b_2$, is delocalized over C−C and C−H bonds with very small contributions from the nitrogens.

Another pattern of overlapping occurs at ∼12.5−12.7 eV. The $\pi_6\ ^2A_2$ cationic state precedes the $\sigma\ ^2A_1$. The latter's MO is chiefly an in-phase combination of nitrogen lone-pair hybrids with some contributions from C−C and C−H σ-bonding lobes. The cationic state corresponding to ionization from a σN_+ combination of nitrogen lone-pair hybrids is at ∼12.7 eV rather than at ∼11 eV.

Ionizations from higher lying σ MOs $20a_1$ (12.9 eV) and $17b_2$ (13.3 eV) correspond to a shoulder in the higher energy region of this large, multistructured band at 12−13.5 eV.

The $\pi-\sigma$ overlap repeats in the higher energy region. Here, the $\pi_7\ ^2B_1$ state precedes the $\sigma\ ^2A_1$. Our calculated energy value agree rather well with the tentative experimental assignment. A low pole strength accompanies the π final state.

The photoelectron spectrum of benzo[*c*]cinnoline has several unusual features. Koopmans's theorem incorrectly predicts the order of the final states. The order of the first two π levels differs from that of phenanthrene. A simple, two-level model does not seem to be applicable to the splitting of nitrogen lone-pair levels in this molecule. Interaction with other σ MOs of identical symmetry generates multiple lone-pair combinations and increases the splitting of the N_- and N_+ levels.

4,7-Phenanthroline. Due to the larger separation of nitrogen nuclei, interaction between lone pairs influences the order of cationic states to a lesser degree than in benzo[*c*]cinnoline. The first two final states have π holes, and the P3 ionization energies are in very good agreement with the experimental values. The amplitude patterns in the corresponding MOs, $4b_1$ and $3a_2$, are similar to those in phenanthrene.

The next two cationic states are very close in energy and correspond to ionization from out-of-phase and in-phase combinations of nitrogen lone-pair hybrids. No splitting is discerned from experiment, and both states are assigned the same energy of 9.5 ± 0.05 eV.[14] Both OVGF and P3 results are in close agreement and produce splittings of 0.05−0.08 eV. The corresponding MOs display significant delocalization over C−N and C−C bonds. Through-bond couplings in the interior of the molecule are manifest in the MOs.

The calculated position of the following ionization band corresponding to the $\pi_3\ ^2A_2$ cationic state is in close agreement with the experimental energy. The same is true for the next two π states, both of B_1 symmetry. The ordering of these states and the electron density patterns do not differ significantly from those in phenanthrene.[13]

The 11.9−12.9 eV region of the experimental spectrum[14] displays a wide, two-hump band. The higher peak was tentatively assigned to ionization from the π_6 level. Our calculations show that both peaks correspond to σ cationic states $^2B_2$ and $^2A_1$, which are placed at 12.2 and 12.6 eV, respectively. Corresponding MOs ($18b_2$ and $20a_1$) display patterns of C−C and C−H bonding (with minor, nitrogen lone-pair contributions in $18b_2$). Appreciable vibronic structure is anticipated for both ionization bands.

According to the present calculations, at least five cationic states are incorporated in a broad, unresolved band at 13−14.5 eV. The first of these, the $\pi_6\ ^2A_2$ state, has a low pole strength and should display significant shake-up structure. Ionization from a σ MO, $17b_2$, follows, and 13.5 eV is predicted for its energy by OVGF and P3. This MO is dominated by C−C and C−H lobes is the external rings, although minor contributions from lone-pair hybrid lobes are present. The following states, $\pi_7\ ^2B_1$ and $\sigma\ ^2A_1$, are very close to each other. One more σ cationic state is included here. All σ orbitals displayed in Figure 5 reveal some contributions from nitrogen lone-pair hybrids.

1,10-Phenanthroline. Because two nitrogen atoms are separated by less than 3 Å, electron correlation has important

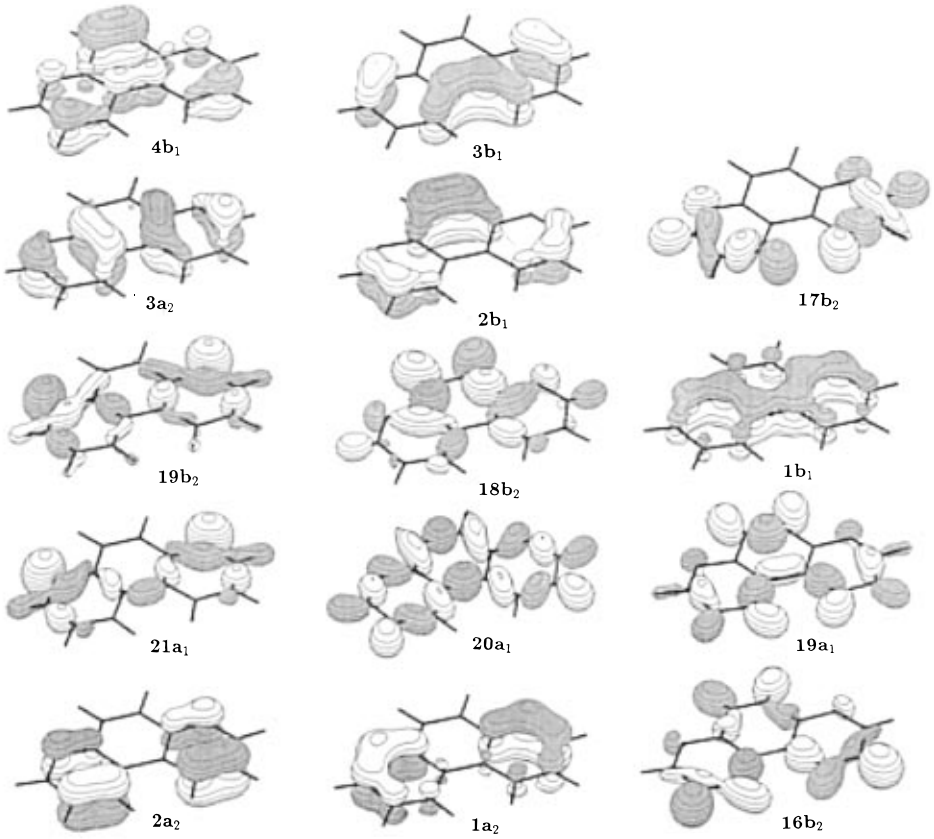

Figure 5. 4,7-Phenanthroline ionization energy FDAs (MOs).

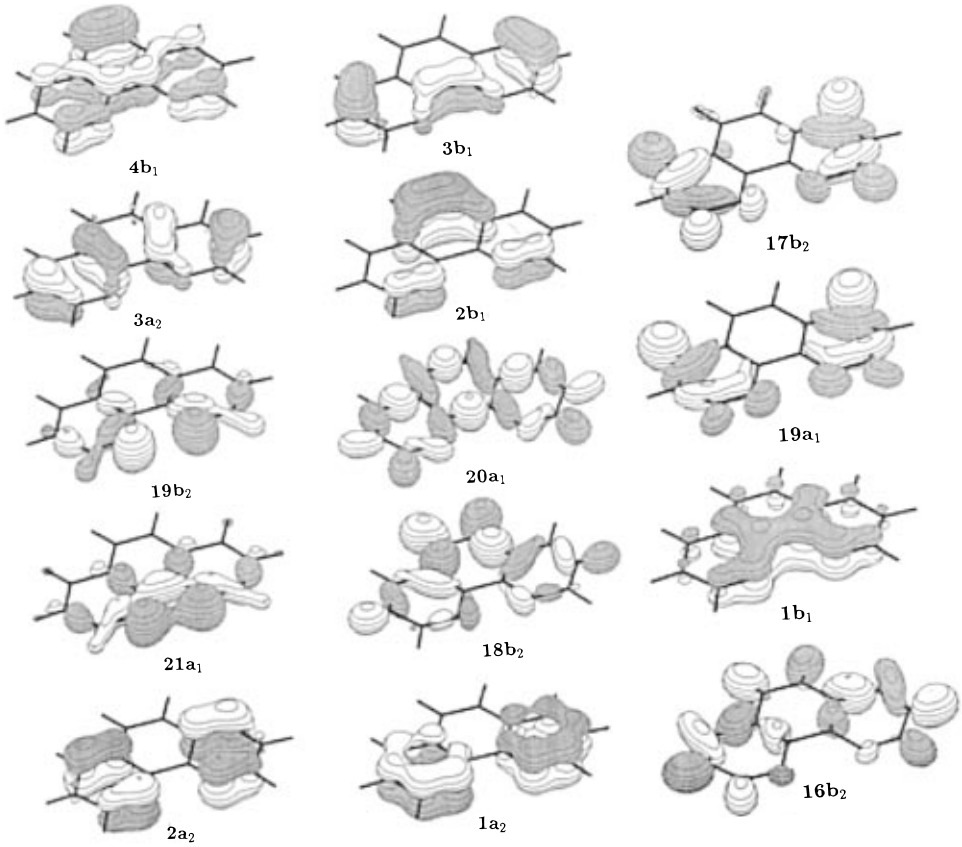

Figure 6. 1,10-Phenanthroline ionization energy FDAs (MOs).

consequences for the order of final states. The first ionization state relates to a π MO with a distribution pattern similar to that of phenanthrene. Both OVGF and P3 energies are very close to the experimental value.[14]

The second ionization band with the experimental maximum at ~8.8 eV represents the overlapping of two cationic states, π_2 $^2A_2$ and the out-of-phase, nitrogen lone-pair hybrid combination, $^2B_2$ (Figure 6). A strong resemblance is obtained between

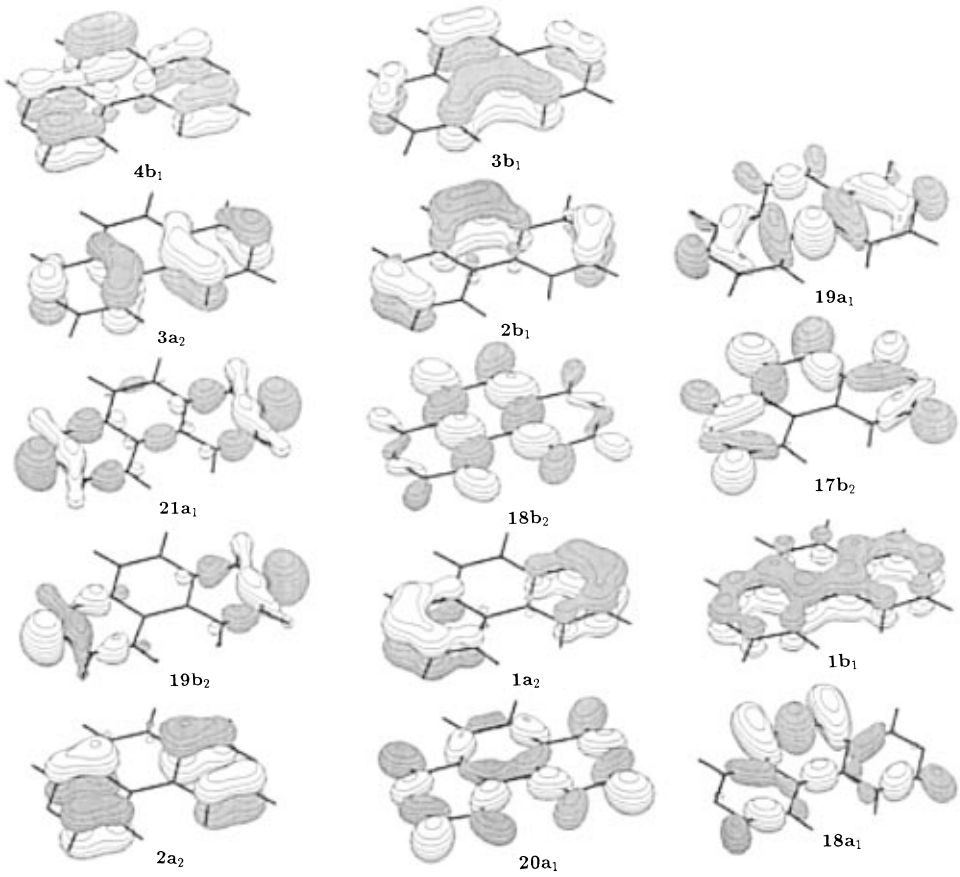

Figure 7. 3,8-Phenanthroline ionization energy FDAs (MOs).

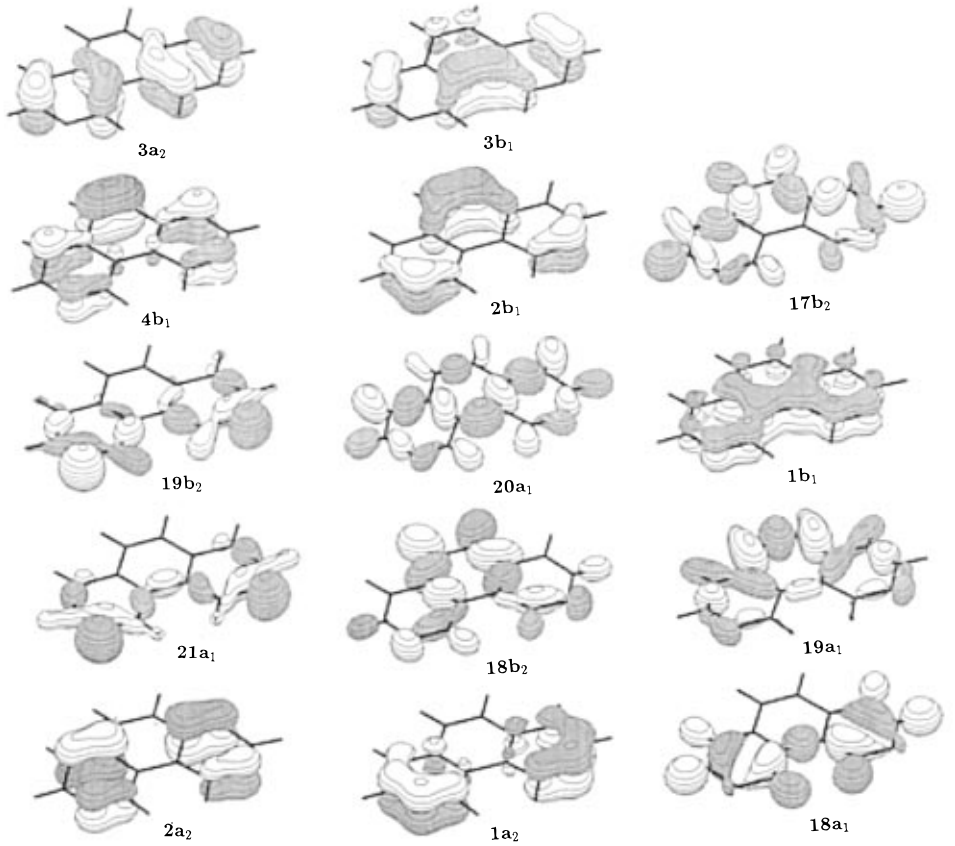

Figure 8. 2,9-Phenanthroline ionization energy FDAs (MOs).

the former's MO and its π_2 counterpart in phenanthrene. The MO $19b_2$, corresponding to the third ionization, while having some C−C bonding character, consists chiefly of nonbonding, lone-pair hybrids. In this case, the MO with an antibonding combination of lone-pair hybrids lies above its bonding counterpart. Ionization energies obtained for these states are 8.49

and 8.89 eV (OVGF) and 8.67 and 8.87 eV (P3), respectively. In the spectrum, there is a large peak at 8.8 eV with a shoulder at 8.6−8.7 eV. Both features are explained by these calculations.

The fourth ionization occurs from an MO dominated by an in-phase combination of lone-pair hybrids, $21a_1$. P3 and OVGF results are in excellent agreement with experiment. An assignment made on the basis of INDO calculations[14] is incorrect. The peak at ∼8.4 eV was assigned to an out-of-phase combination of nitrogen lone-pair hybrids; the in-phase combination was assigned to much higher energy. Our calculations predict the energy splitting of the two lone-pair levels to be only 0.4−0.5 eV and place these levels much closer to the first two π levels. Correlation corrections to Koopmans's theorem must be included in calculations that are performed to interpret this spectrum.

The next three ionizations pertain to π cationic states, and the calculated energies are in good agreement with the experimental values. The order of these π states is the same as in phenanthrene.[13]

Ionization from a σ MO, $20a_1$, follows. Calculated energies correspond satisfactorily with the experimental value, OVGF being closer than the P3 result. There is little nitrogen character in the MO. C−C and C−H σ bonding in $20a_1$ is associated with geometry changes upon ionization and corresponding vibronic structure. A σN_+ state has been assigned to a feature at 11.76 eV.[14] However, the lone-pair contributions are negligible.

Two cationic states contribute to the next ionization band with the experimental maximum at ∼12.4 eV. The first of these, $^2B_2$, corresponds to a σ MO with strong bonding character. As is the case with the preceding σ MO, ionization from this MO ($18b_2$) will lead to significant rearrangement of the nuclear skeleton. The presence of a close-lying $^2A_2$ state with a low pole strength and possible shake-ups further complicates precise assignments for this band.

A wide, unresolved band with apparent vibronic and shake-up structure can be seen at 13.5−14.0 eV. Four more states lie in this energy region. The first two of these are $^2B_2$ and $^2A_1$ σ states corresponding to bonding MOs with some σN_- and σN_+ contributions. Both OVGF and P3 methods predict almost identical splitting for these two MOs. The relative position of the two deepest levels, $1b_1$ and $16b_2$, remains uncertain due to their close energies and a very low pole strength for the former.

3,8-Phenanthroline. No report on the photoelectron spectrum of 3,8-phenanthroline has appeared yet, and this section therefore considers calculations only. The first two ionized states, π_1 $^2B_1$ and π_2 $^2A_2$, will appear at 8.4 and 9.4 eV, respectively. As MOs for these states are nearly the same as their phenanthrene counterparts, the shapes of the bands should resemble those of the first two ionization bands of phenanthrene (Figure 7).

The next two ionizations will occur from two close-lying MOs corresponding to nitrogen lone-pair combinations, the in-phase pattern of $21a_1$ preceding the out-of-phase combination, $19b_2$. The energy gap between these levels is predicted to be 0.1 eV. Related bands are likely to overlap and to appear as one intense peak at ∼9.5 eV.

Ionization from a π_3 $2a_2$ level will probably interfere with the above pattern as the energy of the corresponding cationic state, $^2A_2$, is calculated to be very close.

The next ionized state, π_4 $^2B_1$, is almost 1 eV higher and will be represented by a well-resolved, sharp ionization peak. The related MO displays a distribution pattern very similar to that of the phenanthrene $3b_1$ MO. One may expect this state to occur at 10.9 eV.

The following band at 11.8 eV, corresponding to ionization from $2b_1$, is very likely to overlap with the onset of σ states at 12.0 eV. The resulting feature will probably have shake-up structure due to the low pole strength value for the $^2B_1$ π_5 cationic state. This $\sigma-\pi$ overlapping and shake-up structure pattern will be repeated in the next envelope comprising three ionizations from one π and two σ orbitals at 13.1−13.4 eV. OVGF and P3 give different orderings of states. Because all three corresponding MOs, $1a_2$, $20a_1$, and $19a_1$, are substantially delocalized, significant vibrational structure is anticipated for the ionization band at 13.1−13.4 eV. The latter MO, while consisting mostly of C−C lobes, contains appreciable contributions from an in-phase combination of nitrogen lone-pair hybrids.

The position of the next σ cationic state, $^2B_2$, is predicted at ∼13.7 eV. Delocalized C−C and C−H patterns in the MO will produce significant vibrational structure in the ionization band. Some uncertainty remains for the exact location of the highest π_7 state (∼14.0 eV) due to the low pole strength.

Another σ state with possible vibrational structure is anticipated at 14.4 eV.

2,9-Phenanthroline. In the absence of a published photoelectron spectrum, this section discusses computational results only. As the internuclear separation for two nitrogen atoms in this molecule is almost the same as in the case of 4,7-phenanthroline, one might anticipate almost identical spectral and orbital patterns (Figure 8). Indeed, the orderings of π, σN, and σ states in the calculated spectra of these two phenanthrolines are identical. There are some differences, however. The first two cationic states of 2,9-phenanthroline are predicted to have π holes and to lie at 8.7 and 8.9 eV ($^2A_2$ and $^2B_1$), respectively. These two states are reversed from the first two states in both 4,7-phenanthroline and phenanthrene itself. The energy gap of 0.2−0.3 eV and the possibility of structural changes upon ionization from the latter level will not permit resolution in this part of the photoelectron spectrum. One may expect a pattern different from that for 4,7-phenanthroline. A broad feature with a low-energy shoulder at 8.7 eV, a maximum at 8.9 eV, and a prominent vibrational component at higher energy are predicted to characterize the first two ionizations.

The next two ionizations occur from two orbitals corresponding to out-of-phase ($19b_2$) and in-phase ($21a_1$) combinations of nitrogen lone pairs. Because the energy gap between the two is rather small, ∼0.1 eV, ionization will very likely be displayed as one band at 9.4 eV. The similarity with 4,7-phenanthroline is evident here. Both lone-pair combinations are delocalized over the nearest CC and CH bonds and have higher lying analogs.

The following three ionizations pertain to π states. Although the ordering of these states and distribution patterns in relevant MOs are formally the same as for 4,7-phenanthroline, peak positions and shapes will be different. In the case of 2,9-phenanthroline, the π_3 $^2A_2$ and π_4 $^2B_1$ cationic states are very close and are likely to be displayed as one overlapping band with maxima at 10.4−10.5 eV and no shake-up structure. The third ionization will occur as a separate peak at higher energy, ∼11.9 eV, and is predicted to have shake-up structure.

The onset of σ levels is represented by two very close cationic σ states, $^2A_1$ and $^2B_2$, at 12.5 eV. There will be significant vibrational structure due to the bonding character of MOs $20a_1$ and $18b_2$.

The next band in the PES is very likely to be unresolved, as it will consist of ionizations from very close π_6 ($1a_2$) and σ

($17b_2$) levels at 13.1−13.2 eV. The band structure is predicted to have complicated vibronic structure.

A similar ionization pattern is anticipated in the higher energy region at 14.0 eV with overlapping π_7 and σ cationic states.

The last of the ionizations under consideration will occur from a σ MO, $18a_1$. A band with a maximum at ∼14.6 eV will have significant vibrational structure because of the bonding character of this MO.

Conclusions

P3 and OVGF propagator techniques were applied to photoelectron spectra of polycyclic azaaromatic molecules. Very good agreement between experiemntal He I[14] and calculated vertical ionization energies was achieved. In most cases, P3 values are closer to experiment than OVGF. Because P3 demands smaller computer resources than OVGF, application of this propagator method to large systems is more advantageous. With both methods, correlation corrections for lone-pair holes are very large and reveal numerous defects in the Koopmans ordering of cationic states, especially for phenanthroline isomers. Corresponding orbitals often exhibit significant delocalization between nitrogen, lone-pair hybrids, and σ lobes at C−C and C−H bonding regions. Assignments made on the basis of current calculations provide improved interpretations of existing spectra. Predictions have been made for the photoelectron spectra of 3,8-phenanthroline and 2,9-phenanthroline.

Acknowledgment. This work was supported by the National Science Foundation under Grant CHE-9321434, the Petroleum Research Fund under Grant 29848-AC6, and Gaussian Incorporated.

References and Notes

(1) (a) Acheson, R. M. *Acridines*; Interscience Publishers: New York, 1973. (b) Georghiou, S. *Photochem. Photobiol.* **1977**, *26*, 56. (c) Tanaka, N. *Seitai no Kagaku* **1984**, *35*, 547−549. (d) Tse, H. G.; Comes, M. C. G.; Tse, M. G.; Cesario, M. D.; Medina, H.; Medina, T. *Rev. Cien. Biomed.* **1982**, *3*, 33. (e) Hunt, G. T.; Kindya, R. J.; Hall, R. R. Fennelly, P. F.; Hoyt, M. In *Polynuclear Aromatic Hydrocarbons: Phys. Biol. Chem., Int. Symp.* **1981**, 367.

(2) Swan, G. A. *Phenazines*: Interscience Publishers: New York, 1957.

(3) Mlochowski, J. *Pr. Nauk. Inst. Chem. Org. Fiz. Politech. Wroclaw* **1975**, *9*, 1.

(4) (a) Husseini, R. H.; Stretton, R. *Microbios. Lett.* **1981**, *16*, 85. (b) Weisser, K.; Houngbedji, N. *Cesk. Farm.* **1990**, *39*, 233.

(5) (a) Schilt, A. A. *Analytical Applications of 1,10-Phenanthroline and Related Compounds*; Pergamon Press: Oxford, 1969. (b) Sliwa, W. *Heterocycles* **1979**, *12*, 1207. (c) Cook, M. J.; Lewis, A. P.; McAuliffe, G. S. G. *Org. Magn. Reson.* **1984**, *22*, 388. (d) Nord, G. *Comments Inorg. Chem.* **1985**, *4*, 193.

(6) (a) Barton, J. K. *J. Biomol. Struct. Dyn.* **1983**, *1*, 621. (b) Fleisher, M. B.; Waterman, K. C.; Turro, N. J.; Barton, J. K. *Inorg. Chem.* **1986**, *25*, 3549. (c) Chou, K. C.; Mao, B. *Biopolymers* **1988**, *27*, 1795. (d) Barton, J. K. *NATO ASI Ser., Ser. C* **1989**, *272*, 195. (e) Barton, J. K. *Pure Appl. Chem.* **1989**, *61*, 563. (f) Barton, J. K. *Front. Chem.* **1989**, *1*, 5. (g) Tamilarasan, R.; McMillin, D. R. *Inorg. Chem.* **1990**, *29*, 2798. (h) Veal, J. M.; Rill, R. L. *Biochemistry* **1991**, *30*, 1132. (i) Liu, F.; Meadows, K. A.; McMillin, D. R. *J. Am. Chem. Soc.* **1993**, *115*, 6699. (j) Hasegawa, Y.; Tomito, I. *Trends Inorg. Chem.* **1991**, *2*, 171. (k) Sliwa, W. *Heterocycles* **1994**, *38*, 897. (l) Bassani, D. M.; Wirz, Y.; Hochstrasser, R.; Leupin, W. *J. Photochem. Photobiol., A* **1996**, *100*, 65. (m) Fukui, K.; Tanaka, K. *Nucleic Acids Res.* **1996**, *24*, 3962. (n) Meijler, M. M.; Zelenko, O.; Sigman, D. D. *J. Am. Chem. Soc.* **1977**, *119*, 1135.

(7) (a) Baguley, B. C.; Ferguson, L. R. *Biochem. Pharmacol.* **1986**, *35*, 4581. (b) Satyamoorthy, K.; Chitnis, M. P.; Advani, S. H. *Neoplasma* **1988**, *35*, 27. (c) Byrnes, R. W.; Petering, D. H. *Radiat. Res.* **1993**, *143*, 343. (d) Dzierzbizka, K.; Kolodziejcsyk, A. M.; Sosnowska, D.; Mysliwski, A. *Pept. 1992, Proc. Eur. Pept. Symp. 22nd* **1992**, 889.

(8) (a) Podany, V.; Vachalkova,A.; Bahna, L. *Neoplasma* **1976**, *23*, 617. (b) Ferguson, L. R.; Denny, W. A.; McPhee, D. G. *Mutat. Res.* **1985**, *157*, 29. (c) Hude, W. von der; Behm, C.; Guertler, R.; Basler, H. *Mutat. Res.* **1988**, *203*, 81. (d) Ripley, L. S.; Dubins, J. S.; DeBoer, J. G.; DeMarini, D. M.; Bogert, A. M.; Kreuzer, K. N. *J. Mol. Biol.* **1988**, *200*, 665. (e) Watanabe, T.; Hanasaki, Y.; Hirayama, T.; Fukui, S. *Mutat. Res.* **1989**, *225*, 75. (f) Nakamura, H.; Hase, A.; Funatsuki, K. *Mem. Konan Univ., Sci. Ser.* **1990**, *37*, 177. (g) Ferguson, L. R.; Denny, W. A. *Mutat. Res.* **1991**, *258*, 123.

(9) (a) Okamura, M. Y. *UCLA Symp. Mol. Cell Biol., New Ser.* **1984**, *14*, 381. (b) Takamiya, K.; Iba, K.; Okamura, K. *Biochem. Biophys. Acta* **1987**, *890*, 127. (c) Purugganan, M. D.; Kumar, C. V.; Turro, N. J.; Barton, J. K. *Science* **1988**, *241*, 1645. (d) Lee, G. H.; Della, C. L.; Haim, A. *J. Am. Chem. Soc.* **1989**, *111*, 2535.

(10) (a) Fikus, M.; Golas, T.; Inglot, A. D.; Szulc, B. *Chem.-Biol. Interact.* **1987**, *62*, 25. (b) Mathe, G.; Huppert, J.; Chenu, E.; Bourut, C. *Biomed. Pharmacother.***1989**, *43*, 235. (c) Wilson, W. D.; Ratmeyer, L.; Zhao, H.; Strekowski, L.; Boykin, D. *Biochemistry* **1993**, *32*, 4098. (d) Wilson, W. D.; Ratmeyer, L.; Cegla, M. T.; Spychala, J.; Boykin, D.; Demeunynck, M. *New. J. Chem.* **1994**, *18*, 419. (e) Loya, S.; Bakhanashvili, M.; Tal, R.; Hughes, S. H.; Boyer, P. L.; Hizi, A. *AIDS Res. Hum. Retroviruses* **1994**, *10*, 939. (f) Mazumder, A.; Gupta, M.; Perrin, D. M.; Sigman, D. S.; Rabinovitz, M.; Pommier, Y. *Ibid.* **1995**, *11*, 115.

(11) (a) Singh, P.; Gupta, S. P. *J. Pharm. Sci.* **1978**, *67*, 706. (b) Henry, D. R.; Lavine, B. K.; Jurs, P. C. *Mutat. Res.* **1987**, *179*, 115. (c) Catallo, W. J.; Potier, R. J.; Gale, R. J. *Environ. Toxicol. Water Qual.* **1992**, *7*, 1. (d) Zang, L.; Sanne, K.; Shusterman, A. J.; Hansch, C. *Chem.-Biol. Interact.* **1992**, *81*, 149. (e) Kimura, M. *Trends Heterocycl. Chem.* **1995**, *4*, 103. (f) Barbe, J.; Mandi, Y.; Hever, A.; Petri, I.; Galy, J.-P.; Molnar, J. *In Vivo* **1996**, *10*, 601.

(12) (a) Reinhold, J.; Benedix, R.; Birner, P.; Hennig, H. *Z. Chem.* **1977**, *17*, 115. (b) Barone, V.; Cristinziano, P. L.; Lelj, F.; Pastore, A.; Russo, N. *Gazz. Chim. Ital.* **1982**, *112*, 195. (c) Pal, S. K.; Das Gupta, A.; Das Gupta, N. K. *J. Indian Chem. Soc.* **1987**, *64*, 606. (d) Kao, J. *J. Comput. Chem.* **1988**, *9*, 905. (e) Rak, J.; Blazejowski, J.; Zauhar, R. J. *J. Org. Chem.* **1992**, *57*, 3720. (f) Butler, C. A.; Cooney, R. P. *J. Raman Spectrosc.* **1993**, *24*, 199.

(13) Zakrzewski, V. G.; Dolgounitcheva, O.; Ortiz, J. V. *J. Chem. Phys.* **1996**, *106*, 8748.

(14) Hush, N. S.; Cheung, A. S.; Hilton, P. R. *J. Electron Spectrosc. Relat. Phenom.* **1975**, *7*, 385.

(15) Hoffmann, R.; Imamura, A.; Hehre, W. J. *J. Am. Chem. Soc.* **1968**, *90*, 1499. Adam, W.; Grimison, A. R.; Hoffmann, R. *Ibid.* **1969**, *91*, 2590.

(16) Gleiter, R.; Heilbronner, E.; Hornung, V. *Helv. Chem. Acta* **1972**, *55*, 255. Brogli, F.; Heilbronner, E.; Kobayashi, T. *Ibid.* **1972**, *55*, 274.

(17) Ortiz, J. V.; Zakrzewski, V. G. *J. Chem. Phys.* **1996**, *105*, 2762.

(18) Ortiz, J. V.; Zakrzewski, V. G.; Dolgounitcheva, O. One-Electron Pictures of Electronic Structure: Propagator Calculations on Photoelectron Spectra of Aromatic Molecules. In *Conceptual Trends in Quantum Chemistry, Vol. 3*; Kryachko, E. S., Ed.; Kluwer: Dordrecht, in press.

(19) Ortiz, J. V. In *Computational Chemistry, Reviews of Current Trends, Vol. 2*; Leszczynski, J., Ed.; World Scientific: Singapore, 1997.

(20) Linderberg, L.; Öhrn, Y. *Propagators in Quantum Chemistry*; Academic Press: New York, 1973.

(21) Pickup, B. T.; Goscinski, O. *Mol. Phys.* **1973**, *26*, 1013.

(22) Simons, J. *Theor. Chem. Adv. Persp.* **1978**, *3*, 1.

(23) Herman, M. F.; Freed, K. F.; Yeager, D. L. *Adv. Chem. Phys.* **1981**, *48*, 1.

(24) Öhrn, Y.; Born, G. *Adv. Quantum Chem.* **1981**, *13*, 1.

(25) Niessen, W. von; Schirmer, J.; Cederbaum, L. S. *Comput. Phys. Rep.* **1984**, *1*, 57.

(26) Ortiz, J. V. *J. Chem. Phys.* **1996**, *104*, 7599.

(27) Dunning, T. H. *J. Chem. Phys.* **1989**, *90*, 1007.

(28) Total energies for the molecules under consideration (cc-pVDZ): acridine, −552.03723 au; phenazine, −568.02976 au; benzo[*c*]cinnoline, −568.002215 au; 4,7-phenanthroline, −568.04180 au; 1,10-phenanthroline, −568.03706 au; 3,8-phenanthroline, −568.03742 au; 2,9-phenanthroline, −568.03629 au.

(29) Krishnan, R.; Binkley, J. S.; Seeger, R.; Pople, J. A. *J. Chem. Phys.* **1980**, *72*, 650.

(30) Frisch, M. J.; Trucks, G. W.; Schlegel, H. B.; Gill, P. M. W.; Johnson, B. G.; Robb, M. A.; Cheeseman, J. R.; Keith, T. A.; Petersson, G. A.; Montgomery, J. A.; Raghavachari, K.; Al-Laham, M. A.; Zakrzewski, V. G.; Ortiz, J. V.; Foresman, J. B.; Cioslowski, J.; Stefanov, B. B.; Nanayakkara, A.; Challacombe, M.; Peng, C. Y.; Ayala, P. Y.; Chen, W.; Wong, M. W.; Andres, J. L.; Replogle, E. S.; Gomperts, R.; Martin, R. L.; Fox, D. J.; Binkley, J. C.; Defrees, D. J.; Baker, J.; Stewart, J. J. P.; Head-Gordon, M.; Gonzalez, C.; Pople, J. A. *GAUSSIAN 94, Revision B.3*; Gaussian, Inc.: Pittsburgh, PA, 1995.

(31) Schaftenaar, G. *MOLDEN*, CAOS/CAMM Center: The Netherlands, 1991.

(32) Zakrzewski, V. G.; Ortiz, J. V.; Nichols, J. A.; Heryadi, D.; Yeager, D. L.; Golab, T. *Int. J. Quantum Chem.* **1996**, *60*, 29.

(33) Zakrzewski, V. G.; Ortiz, J. V. *Int. J. Quantum Chem., Quantum Chem. Symp.* **1994**, *28*, 23. Zakrzewski, V. G.; Ortiz, J. V. *Int. J. Quantum Chem.* **1995**, *53*, 583.

(34) Zakrzewski, V. G.; Ortiz, J. V. *J. Phys. Chem.* **1996**, *100*, 13979.

(35) Zakrzewski, V. G.; Ortiz, J. V. *J. Mol. Struct. (THEOCHEM)* **1996**, *388*, 351.

(36) Zakrzewski, V. G.; Dolgounitcheva, O.; Ortiz, J. V. *J. Chem. Phys.* **1996**, *106*, 5872.